Journal of Magnetic Resonance **150,** 10–16 (2001)
doi:10.1006/jmre.2001.2311, available online at http://www.idealibrary.com on IDEAL®

Determination of Quadrupole Parameters with a Composite Pulse for Spurious Signal Suppression

Y. Millot and P. P. Man

Laboratoire de Chimie des Surfaces, CNRS FRE 2312, Systèmes Interfaciaux à l'Echelle Nanométrique, Université Pierre et Marie Curie, 4 Place Jussieu, Tour 55, Casier 196, 75252 Paris Cedex 05, France

Received May 8, 2000; revised February 13, 2001; published online April 17, 2001

Spurious signals such as the piezoelectric signal from a ferroelectric crystal or the ringing signal from the NMR probe head tuned for low gyromagnetic ratio nuclei are often observed in pulsed NMR. Both signals are cancelled using the Hahn echo sequence with appropriate phase cyclings. The present paper applies a composite-pulse sequence to cancel the ringing signal. The main advantage of this sequence over the Hahn echo sequence is in the simplicity of optimizing the line intensity: the optimization of only one pulse duration for this sequence but of two pulse durations and the interpulse delay for the Hahn echo sequence. We are interested in half-integer quadrupole spins ($I = \frac{3}{2}, \frac{5}{2}, \frac{7}{2}$, and $\frac{9}{2}$), which means that we must consider the first-order quadrupole interaction during the pulses. For simplicity, we deal mainly with spin $I = \frac{3}{2}$ nuclei. Since the central-line intensity depends on the ratio of the quadrupole coupling constant (QCC) to the amplitude of the RF pulse, we can determine the QCC from a featureless lineshape by fitting the variation of the experimental central-line intensity for increasing pulse duration with theoretical results. Contrary to the one-pulse sequence where the central-line intensity is proportional to the pulse duration if the latter is short, there is no such condition with the composite-pulse sequence. In other words, this sequence does not allow us to quantify the relative spin populations in powders. The size of the sample must be much smaller than that of the RF coil in order for the RF magnetic field to become homogeneous for the sample. We used ^{87}Rb ($I = \frac{3}{2}$) in an aqueous solution of RbCl and in $RbNb_2O_5F$ powder, ^{131}Xe ($I = \frac{3}{2}$) of xenon gas physisorbed in Na–Y zeolite, and ^{23}Na ($I = \frac{3}{2}$) in two well-known powders ($NaNO_3$ and $NaNO_2$) to support our theoretical result.

Key Words: **spurious signal suppression; half-integer quadrupole spin; composite-pulse sequence; featureless lineshape; spin-population quantification.**

INTRODUCTION

In pulsed NMR, spurious signals are often observed with the one-pulse sequence (Fig. 1a) as a complex FID superimposed on that of the spin system (*1, 2*). They distort the spectra so strongly that the lineshape becomes difficult to recognize. There are two kinds of spurious signals: (i) the ringing signals from the NMR probe head tuned for low gyromagnetic ratio nuclei in strong Zeeman field B_0 and (ii) the piezoelectric signals from ferroelectric materials in single crystal form (*3, 4*). Figure 2a presents the effects of the ringing on the spectra of ^{131}Xe ($I = \frac{3}{2}$) of xenon gas, physisorbed in the supercages of Na–Y zeolite, for increasing pulse duration t_1. Clearly, we have difficulty recognizing the ^{131}Xe lineshape.

The two-pulse Hahn echo sequence with appropriate phase cyclings cancels these spurious signals (*1, 5, 6*). However, the use of this sequence requires the optimization of the durations of the two pulses and of the interpulse delay for obtaining the best line intensity. We apply a composite-pulse sequence consisting of three pulses of the same duration t_1 but without any delay between them (Fig. 1b) and with the following four phase cyclings (*7*):

First RF pulse:	$-X$	$-X$	$+X$	$+X$	
Second RF pulse:	$+X$	$+X$	$+X$	$+X$	[Sequence 1]
Third RF pulse:	$+X$	$-X$	$-X$	$+X$	
Receiver:	$+X$	$-X$	$+X$	$-X$.	

With the one-pulse sequence, an acquisition delay d (Fig. 1) of 80 μs is necessary to not detect the ringing signals for ^{131}Xe FIDs. In contrast, only a $d = 20$ μs is required with this composite-pulse sequence to observe ^{131}Xe FIDs without any ringing signals, resulting in flat-baseline spectra (Fig. 2b).

The present paper applies this composite-pulse sequence to determine the two quadrupole parameters of half-integer quadrupole spins ($I = \frac{3}{2}, \frac{5}{2}, \frac{7}{2}$, and $\frac{9}{2}$) in powder: the quadrupole coupling constant e^2qQ/h (QCC) and the asymmetry parameter η. For simplicity we focus on a spin $I = \frac{3}{2}$ system in powder. If the second-order quadrupole interaction $H_Q^{(2)}$ is present, the central-transition lineshape acquired with one-pulse, the composite-pulse, or the Hahn echo sequences should provide us with the QCC and η (*1, 8, 9*). However, if $H_Q^{(2)}$ is small, the first-order quadrupole interaction $H_Q^{(1)}$ becomes the main internal interaction. As a result, the spectrum of the central line has a featureless lineshape, which means that the lineshape analysis is not useful for determining QCC and η. We can apply the 2D nutation approach to find the two quadrupole parameters (*10, 11*). Due to the long pulse duration involved in this

1090-7807/01 $35.00

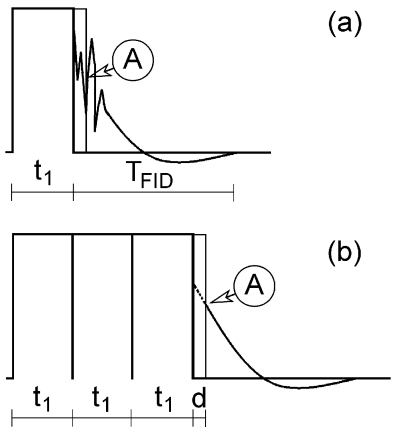

FIG. 1. (a) One-pulse sequence whose pulse duration is t_1 and (b) composite-pulse sequence whose total pulse duration is $3t_1$. Due to the acquisition delay d, the FID acquisition, whose duration is T_{FID}, starts at point A.

experiment, we prefer to apply the 1D nutation approach with the composite-pulse sequence and extract the QCC by fitting the experimental line intensity for increasing pulse duration with the theoretical expression and the Simplex procedure.

We take into account $H_{\mathrm{Q}}^{(1)}$ during the RF pulses (*11–16*) because the quadrupole coupling ω_{Q} can be bigger than the amplitude ω_{RF} of the RF pulse. In the literature, considering $H_{\mathrm{Q}}^{(1)}$ during the RF pulses is called soft-pulse excitation. On the other hand, if $H_{\mathrm{Q}}^{(1)}$ is neglected during the RF pulses, the excitation is called hard-pulse excitation. Of course, the soft-pulse excitation includes the hard-pulse case. Consequently, our theoretical results on line intensity are valid for any ratio of $\omega_{\mathrm{Q}}/\omega_{\mathrm{RF}}$ for single crystals or QCC/ω_{RF} for powders. However, there is an upper limit for these ratios over which the theoretical line intensity does not change anymore. In contrast to the one-pulse sequence, numerical calculation on the central-line intensity generated by this composite-pulse sequence shows that there is no excitation condition (the pulse duration t_1) that allows us to quantify relative spin populations in powder. We illustrate the two extreme cases (zero QCC) with the nuclei ^{87}Rb ($I = \frac{3}{2}$) in an aqueous solution of RbCl where the electric-field gradient (EFG) is zero and in Pyrochlore $RbNb_2O_5F$ powder where the EFG is strong (*17*). For intermediate cases we use the nuclei ^{23}Na ($I = \frac{3}{2}$) in two extensively studied compounds, $NaNO_3$ and $NaNO_2$, whose e^2qQ/h and η are (0.336 MHz, 0.0) and (1.1 MHz, 0.1), respectively (*18–20*).

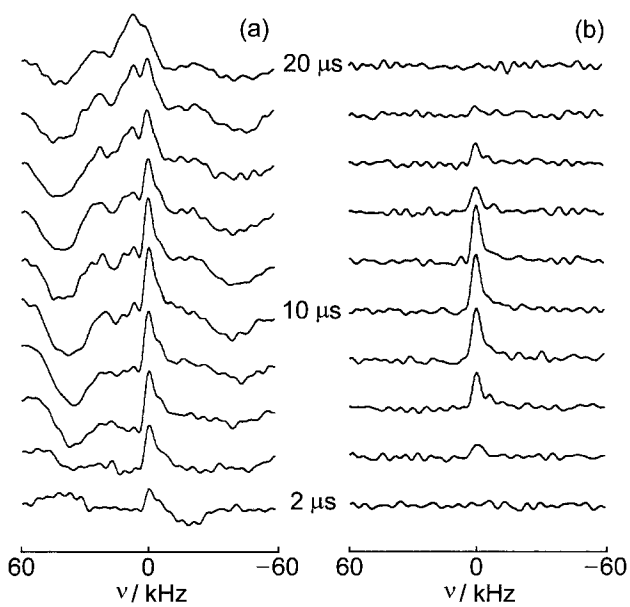

FIG. 2. (a) ^{131}Xe one-pulse spectra and (b) composite-pulse spectra of xenon physisorbed on Na–Y zeolite, for increasing t_1 ranging from 2 to 20 μs in steps of 2 μs. Xenon pressure is 700 Torr. FIDs were acquired with $d = 20$ μs; NS = 2800; $D_0 = 0.3$ s.

THEORY

The Hamiltonians throughout the paper are defined in angular frequency units. Considering only the first-order quadrupole interaction $H_{\mathrm{Q}}^{(1)}$ and neglecting magnetic dipole–dipole couplings, chemical shift anisotropy, and relaxation phenomena, the Hamiltonian during an X pulse is

$$H^{(x)} = H_{\mathrm{Q}}^{(1)} - \omega_{\mathrm{RF}} I_x; \qquad [1]$$

that during a $-X$ pulse is

$$H^{(-x)} = H_{\mathrm{Q}}^{(1)} + \omega_{\mathrm{RF}} I_x, \qquad [2]$$

with

$$H_{\mathrm{Q}}^{(1)} = \frac{1}{3}\omega_{\mathrm{Q}}\left[3I_z^2 - I(I+1)\right], \qquad [3]$$

$$\omega_{\mathrm{Q}} = \frac{3e^2qQ}{8I(2I-1)\hbar}[3\cos^2\beta - 1 + \eta\sin^2\beta\cos 2\alpha]. \qquad [4]$$

The first two Euler angles α and β describe the orientation of the Zeeman field B_0 in the principal axis system (PAS) of the EFG tensor. The quadrupole coupling ω_{Q} is defined experimentally as half the frequency separating two consecutive lines in the spectrum of a single crystal.

The dynamics of a quadrupole spin system excited by the composite-pulse sequence is described by four density operators $\rho_1(3t_1)$, $\rho_2(3t_1)$, $\rho_3(3t_1)$, and $\rho_4(3t_1)$ associated with the four phase cyclings in Sequence [1]:

$$\begin{aligned}\rho_1(3t_1) &= \exp\left(-2iH^{(x)}t_1\right)\exp\left(-iH^{(-x)}t_1\right)\rho(0)\\ &\quad\times\exp\left(iH^{(-x)}t_1\right)\exp\left(2iH^{(x)}t_1\right)\\ &= \exp\left(-2iH^{(x)}t_1\right)\rho_{-x}(t_1)\exp\left(2iH^{(x)}t_1\right) \qquad [5]\end{aligned}$$

for the first acquisition of the FID,

$$\begin{aligned}\rho_2(3t_1) &= \exp\left(-iH^{(-x)}t_1\right)\exp\left(-iH^{(x)}t_1\right)\exp\left(-iH^{(-x)}t_1\right)\\ &\quad\times\rho(0)\exp\left(iH^{(-x)}t_1\right)\exp\left(iH^{(x)}t_1\right)\exp\left(iH^{(-x)}t_1\right)\\ &= \exp\left(-iH^{(-x)}t_1\right)\exp\left(-iH^{(x)}t_1\right)\rho_{-x}(t_1)\\ &\quad\times\exp\left(iH^{(x)}t_1\right)\exp\left(iH^{(-x)}t_1\right) \qquad [6]\end{aligned}$$

for the second FID acquisition,

$$\begin{aligned}\rho_3(3t_1) &= \exp\left(-iH^{(-x)}t_1\right)\exp\left(-2iH^{(x)}t_1\right)\\ &\quad\times\rho(0)\exp\left(2iH^{(x)}t_1\right)\exp\left(iH^{(-x)}t_1\right)\\ &= \exp\left(-iH^{(-x)}t_1\right)\rho_x(2t_1)\exp\left(iH^{(-x)}t_1\right) \qquad [7]\end{aligned}$$

for the third acquisition, and

$$\begin{aligned}\rho_4(3t_1) &= \exp\left(-3iH^{(x)}t_1\right)\rho(0)\exp\left(3iH^{(x)}t_1\right)\\ &= \rho_x(3t_1) \qquad [8]\end{aligned}$$

for the last acquisition. In Eqs. [5]–[8], the density operators of the first pulse are introduced: $\rho_x(t_1)$ and $\rho_{-x}(t_1)$ for an X pulse and a $-X$ pulse of pulse duration t_1, whose expressions are

$$\rho_x(t_1) = \exp\left(-iH^{(x)}t_1\right)\rho(0)\exp\left(iH^{(x)}t_1\right), \qquad [9]$$

$$\rho_{-x}(t_1) = \exp\left(-iH^{(-x)}t_1\right)\rho(0)\exp\left(iH^{(-x)}t_1\right). \qquad [10]$$

In the high temperature approximation, the thermodynamic equilibrium state is described by $\rho(0) = I_z$. The central-line intensity $S(3t_1)$ is given by

$$S(3t_1) = \left\langle -\frac{1}{2}\middle|\{\rho_1(3t_1) - \rho_2(3t_1) + \rho_3(3t_1) - \rho_4(3t_1)\}\middle|\frac{1}{2}\right\rangle, \qquad [11]$$

where the signs of the four density operators $\pm\rho_j(3t_1)$ are those of the receiver phase given in Sequence [1]. Similarly, for the one-pulse sequence, the central-line intensity is given by

$$S(t_1) = \left\langle -\frac{1}{2}\middle|\rho_x(t_1)\middle|\frac{1}{2}\right\rangle. \qquad [12]$$

In fact, Eqs. [5]–[10] are defined by quantum operators. In practice, they are expressed in matrix form in order to apply matrix multiplication, which can be performed by computer. Since the matrices of $H^{(x)}$ and $H^{(-x)}$ expressed in the eigenstates of I_z are not diagonal, the matrices of their eigenvalues and eigenvectors must be determined first. The two Hamiltonians $H^{(x)}$ and $H^{(-x)}$ have the same eigenvalue matrix Ω, but different eigenvector matrices, denoted by T and U, respectively. Analytical expressions for Ω, T, and U were obtained for a spin $I = \frac{3}{2}$ system (*21*). However, it is easier to determine them with numerical procedures, which are valid for the four half-integer quadrupole spins. For the first X or $-X$ pulses of the composite sequence, the density operators become

$$\rho_x(t_1) = T\exp(-i\Omega t_1)T^\dagger\,\rho(0)T\exp(i\Omega t_1)T^\dagger, \qquad [13]$$

$$\rho_{-x}(t_1) = U\exp(-i\Omega t_1)U^\dagger\,\rho(0)U\exp(i\Omega t_1)U^\dagger. \qquad [14]$$

Since the density operator $\rho(t_1, \varphi)$ associated with an RF pulse of phase φ (phase relative to that of an X-pulse) is related to that of an X-pulse $\rho_x(t_1)$ by

$$\rho(t_1, \varphi) = \exp(-i\,\varphi\,I_z)\rho_x(t_1)\exp(i\,\varphi\,I_z), \qquad [15]$$

in the matrix form, an element of $\rho(t_1, \varphi)$ and that corresponding to $\rho_x(t_1)$ are related by

$$\langle r|\rho(t_1, \varphi)|c\rangle = \langle r|\rho_x(t_1)|c\rangle\exp(-ip\varphi), \qquad [16]$$

p being the coherence order (*22*). Equation [15] allows us to rewrite Eqs. [5]–[8] as

$$\rho_1(3t_1) = T\exp(-2i\Omega t_1)T^\dagger\rho(t_1, \pi)T\exp(2i\Omega t_1)T^\dagger, \qquad [17]$$

$$\begin{aligned}\rho_2(3t_1) &= U\exp(-i\Omega t_1)U^\dagger T\exp(-i\Omega t_1)T^\dagger\,\rho(t_1, \pi)\\ &\quad\times T\exp(i\Omega t_1)T^\dagger U\exp(i\Omega t_1)U^\dagger, \qquad [18]\end{aligned}$$

$$\rho_3(3t_1) = U\exp(-i\Omega t_1)U^\dagger\rho_x(2t_1)U\exp(i\Omega t_1)\,U^\dagger, \qquad [19]$$

$$\rho_4(3t_1) = \rho_x(3t_1). \qquad [20]$$

Equations [17]–[20] require numerous matrix multiplications. For this reason we perform a numerical calculation instead of an analytical calculation. For powdered samples, averaging the direction of B_0 in the PAS of the EFG tensor is performed according to the previously described procedure (*18, 23*). The averaged central-line intensities are denoted by $\langle S(t_1)\rangle$ and $\langle S(3t_1)\rangle$ for the one-pulse and the composite-pulse sequences, respectively. They depend on t_1, ω_{RF}, e^2qQ/h, and η, instead of on t_1, ω_{RF}, ω_Q, and η for the central-line intensities $S(t_1)$ and $S(3t_1)$ of a single crystal. Experimentally, the central-line intensity is given by the amplitude of the first sampled point of the FID or the integrated area of the central line; both are affected by the acquisition delay d.

Figure 3a presents the graphs of the averaged central-line intensity $\langle S(t_1)\rangle$ of a spin $I = \frac{3}{2}$ system versus the pulse duration t_1 in the one-pulse sequence. Several QCCs, always with $\eta = 0$, have been used. The graphs have sine shapes. In fact, they are the sum of sine curves with different amplitudes and phases. These properties are the foundation of the 2D nutation approach (*11*). The Fourier transform of these sine curves provides us with a specific lineshape in the F_1 dimension of 2D nutation spectrum. This lineshape depends on the QCC/ω_{RF} ratio and η. Figure 3a shows that the maximum of the line intensity and the associated pulse duration decrease when the QCC increases (*14, 15, 20*).

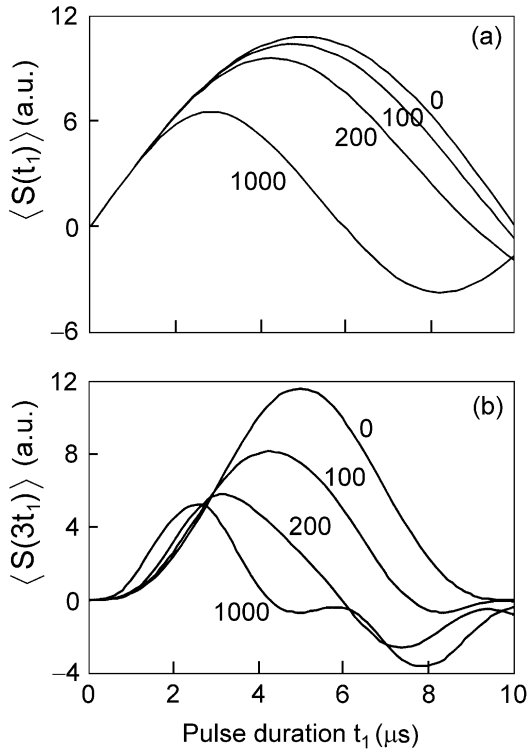

FIG. 3. Calculated powder central-line intensities of a spin $I = \frac{3}{2}$, (a) $\langle S(t_1)\rangle$ for the one-pulse sequence and (b) $\langle S(3t_1)\rangle$ for the composite-pulse sequence, with the pulse duration t_1 ranging from 0 to 10 μs for four values of e^2qQ/h (0, 100, 200, and 1000 kHz); $\eta = 0$; $\omega_{RF}/(2\pi) = 50$ kHz.

However, for short pulse duration, the line intensity is proportional to the pulse duration t_1, whatever the QCC. This is the well-known excitation condition for obtaining quantitative results on the spin population in powder. Figure 3b presents the graphs of the central-line intensity $\langle S(3t_1)\rangle$ of a spin $I = \frac{3}{2}$ system versus the pulse duration t_1 of the composite-pulse sequence with the same parameters as for the one-pulse sequence. The graph for $e^2qQ/h = 0$ is a bell-shape curve and that for $e^2qQ/h = 1$ MHz has two bell shapes of opposite signs. As with the one-pulse sequence (Fig. 2a), the pulse duration that maximizes the central-line intensity in the selective excitation condition ($e^2qQ/h \gg \omega_{RF}/(2\pi)$) is half that corresponding to the nonselective excitation condition ($e^2qQ/h \ll \omega_{RF}/(2\pi)$). The first maximum of the central-line intensity and the corresponding pulse duration decrease when the QCC increases. But there is no linear regime where the line intensity is proportional to the pulse duration, even for short pulse duration. In other words, quantitative results on spin populations are not possible with this composite-pulse sequence. The three curves concerning $e^2qQ/h = 0,\ 100$, and 200 kHz (Fig. 3a) are similar for the one-pulse sequence. In contrast, the corresponding three curves for the composite-pulse sequence (Fig. 3b) are much more distinguishable. As a result, the 1D nutation approach with the composite-pulse sequence allows a precise determination of weak e^2qQ/h values.

In practice, the FID acquisition starts at point A (Fig. 1). Therefore, the first part of the FID is lost. As long as d is small compared to the duration T_{FID} of the FID, d has a negligible effect on the spectra. This is the case for ^{131}Xe of xenon gas physisorbed on Na–Y zeolite at room temperature where motion averages the EFG in the supercages (Fig. 2b). However, in general, the lines of solids are broad and an important part of the FID can be lost. The spin-echo sequence is recommended in this case to recover the lost part of the FID (*1*).

EXPERIMENTAL AND RESULTS

The FIDs were recorded at room temperature with a Bruker MSL 400 multinuclear high-power pulsed NMR spectrometer. The resonance frequencies of ^{131}Xe, ^{23}Na, and ^{87}Rb are 32.8, 105.80, and 130.88 MHz, respectively. The high-power static probe head was equipped with a solenoid coil 10 mm in diameter and 35 mm in length. In order to have a homogeneous RF field B_1, a spherical container was used for aqueous solutions; on the other hand, powdered samples were packed as a cylinder 5 mm high and centered in the solenoid coil. Other experiment details are given in the figure legends, namely, the number of scans (NS), the recycle delay (D_0), the acquisition delay or the dead time of the receiver (d), and the RF pulse amplitude ω_{RF}.

Figures 4a and 4b show two series of ^{87}Rb spectra of an aqueous solution of RbCl versus the pulse duration, acquired with the one-pulse and the composite-pulse sequences, respectively.

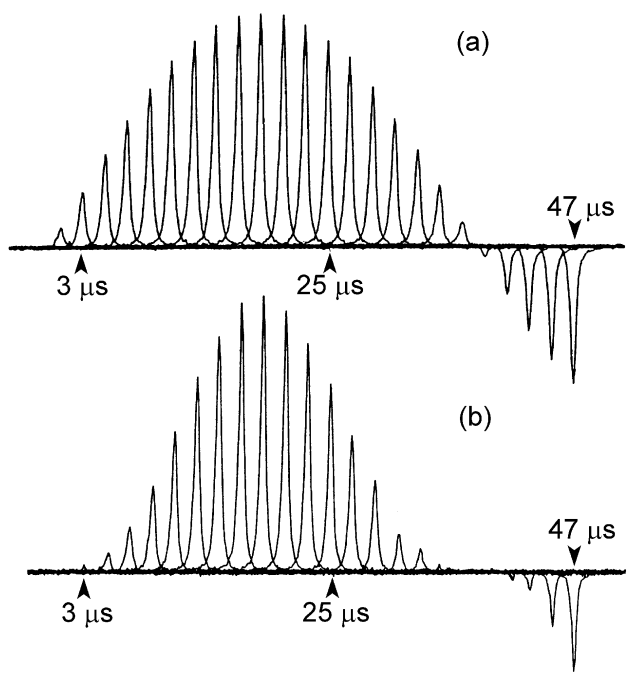

FIG. 4. ^{87}Rb spectra of an aqueous solution of RbCl, obtained from the one-pulse sequence (a) and from the composite-pulse sequence (b), with the pulse duration t_1 ranging from 1 to 47 μs in steps of 2 μs; $D_0 = 2$ s; $d = 20$ μs; NS = 4.

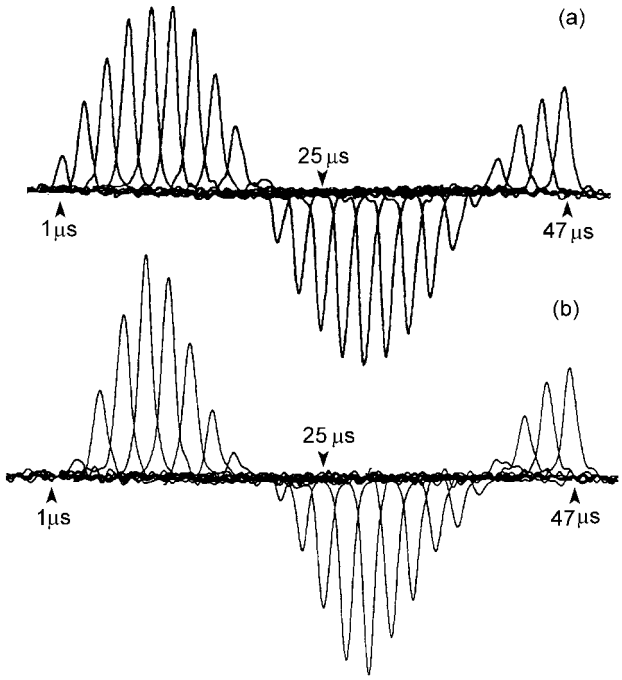

FIG. 5. ^{87}Rb spectra of powdered Pyrochlore $RbNb_2O_5F$, obtained from the one-pulse sequence (a) and from the composite-pulse sequence (b), with the pulse duration t_1 ranging from 1 to 47 μs in steps of 2 μs; $D_0 = 1$ s; $d = 20$ μs; NS = 64.

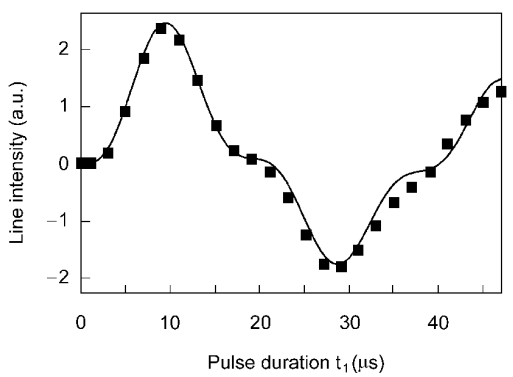

FIG. 6. Fit (solid line) of $^{87}RbNb_2O_5F$ experimental line intensities (filled squares) from Fig. 5b with $I = \frac{3}{2}$, $e^2qQ/h = 324$ kHz, $\eta = 0$, and $\omega_{RF}/(2\pi) = 13.53$ kHz.

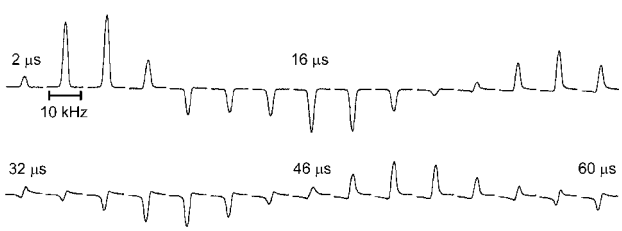

FIG. 7. ^{23}Na spectra of powdered $NaNO_3$, obtained from the composite-pulse sequence, with the pulse duration t_1 ranging from 2 to 60 μs in steps of 2 μs; $D_0 = 100$ s; $d = 6$ μs; NS = 16; $\omega_{RF}/(2\pi) = 23.31$ kHz.

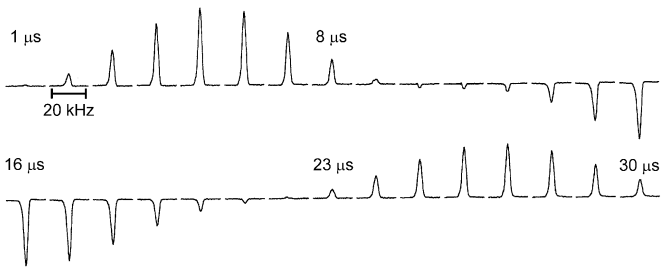

FIG. 8. ^{23}Na spectra of powdered $NaNO_2$, obtained from the composite-pulse sequence, with the pulse duration t_1 ranging from 1 to 30 μs in steps of 1 μs; $D_0 = 1$ s; $d = 6$ μs; NS = 64; $\omega_{RF}/(2\pi) = 23.31$ kHz.

Since the EFG is averaged to zero in aqueous solution, the line intensity is similar to the "averaged" central-line intensities. Its behavior versus the pulse duration is in agreement with simulated curves in Figs. 3a and 3b corresponding to $e^2qQ/h = 0$. For the one-pulse sequence, the curve has a sine shape; for the composite-pulse sequence, the curve is bell-shaped. The pulse duration given the highest signal is 21 μs, which means that the RF pulse amplitude is $\omega_{RF}/(2\pi) = 12$ kHz. Figures 5a and 5b show two series of ^{87}Rb spectra of Pyrochlore $RbNb_2O_5F$ versus the pulse duration, acquired with the one-pulse and the composite-pulse sequences, respectively. The variation of the averaged central-line intensities versus the pulse duration is in agreement with the prediction. Indeed, the pulse duration (t_1=10 μs) that maximizes the line intensity is nearly half that determined with the aqueous solution ($t_1 = 21$ μs). Figure 6 shows the best fit of the experimental line intensities of Fig. 5b with $I = \frac{3}{2}$, $\omega_{RF}/(2\pi) = 13.53$ kHz, $\eta = 0$, and $e^2qQ/h = 324$ kHz. The fit is not perfect; only half of the experimental data are on the calculated curve. The RF pulse amplitude is higher than that of the experimental one by 1.53 kHz. Increasing the QCC value does not change the curve because the limit of strong QCC value is reached, strong relative to the value of the RF pulse amplitude. The QCC/ω_{RF} ratio is 27; that corresponding to Fig. 3b is 20. The lower limit for the QCC of ^{87}Rb in this sample should be 324 kHz. A more accurate

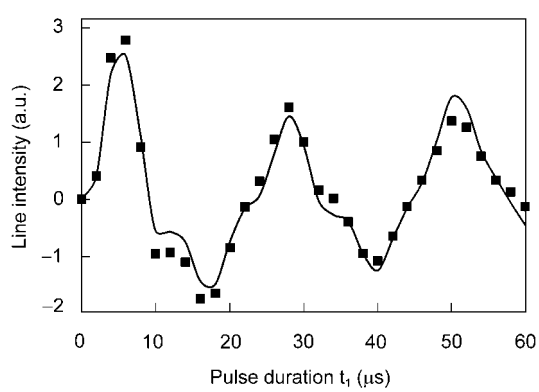

FIG. 9. Fit (solid line) of $^{23}NaNO_3$ experimental line intensities (filled squares) from Fig. 7 with $I = \frac{3}{2}$, $e^2qQ/h = 354$ kHz, $\eta = 0$, and $\omega_{RF}/(2\pi) = 23.37$ kHz.

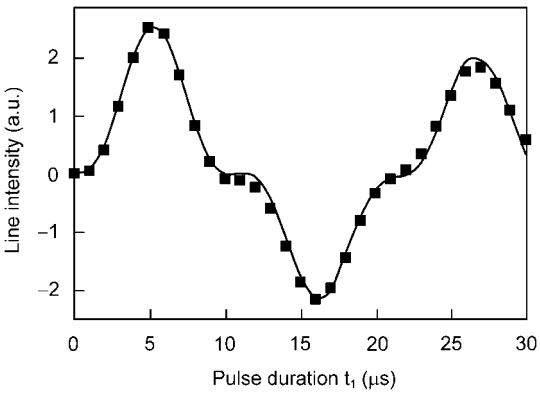

FIG. 10. Fit (solid line) of $^{23}NaNO_2$ experimental line intensities (filled squares) from Fig. 8 with $I = \frac{3}{2}$, $e^2qQ/h = 995$ kHz, $\eta = 0$, and $\omega_{RF}/(2\pi) = 23.62$ kHz.

determination of QCC should be obtained with a stronger RF pulse amplitude using a smaller RF coil.

The above two examples illustrate well the two excitation conditions: the nonselective excitation (Figs. 4a and 4b) and the selective excitation (Figs. 5a and 5b). The following two examples (^{23}Na in $NaNO_3$ and $NaNO_2$) with well-defined quadrupole parameters allow us to test our fitting program. The RF pulse amplitude for ^{23}Na, determined with the same methods as ^{87}Rb, is $\omega_{RF}/(2\pi) = 23.31$ kHz. Figures 7 and 8 show the variation of the ^{23}Na spectra of $NaNO_3$ and $NaNO_2$ with the pulse duration acquired with the composite-pulse sequence. Figure 9 shows the fit of the experimental line intensities of Fig. 7 with $I = \frac{3}{2}$, $\omega_{RF}/(2\pi) = 23.37$ kHz, $\eta = 0$, and $e^2qQ/h = 354$ kHz. Figure 10 shows the fit of the experimental line intensities of Fig. 8 with $I = \frac{3}{2}$, $\omega_{RF}/(2\pi) = 23.62$ kHz, $\eta = 0$, and $e^2qQ/h = 995$ kHz. Due to the small size of the samples compared to that of the RF coil, the RF magnetic field is homogeneous, resulting a good agreement between experimental and fit values of $\omega_{RF}/(2\pi)$ and of e^2qQ/h. The last two examples show that our approach to determining the QCC is reliable and that our fitting program is efficient.

CONCLUSIONS

The powder averaged central-line intensity for the spin $I = \frac{3}{2}$ system excited by the composite pulse for spurious signal suppression has been investigated by taking into account the first-order quadrupole interaction during the RF pulses. The simplicity of this sequence over the Hahn echo sequence to cancel the ringing signal is obvious: only one parameter (the pulse duration) must be optimized. For a featureless central lineshape, fitting the line intensity against the pulse duration allows us to determine the QCC. This composite pulse is efficient for determining weak QCC values, that is, the width of the featureless lineshape should be of few kilohertz. Our theoretical results and most of our experimental ones deal with $\eta = 0$ because the central line has a featureless shape; in fact, we should consider a nonzero value for η to fit the experimental line intensity. Our approach remains valid for the other half-integer quadrupole spins. Despite the fact that this sequence cancels the ringing signals with an acquisition delay of the same order of magnitude as that for high gyromagnetic ratio nuclei, spectra with broad lines or short FIDs are still distorted by this acquisition delay. The spin-echo should be used to recover signals lost in the acquisition delay. The main drawback of this 1D nutation method is the restriction to a single QCC determination. If this is not the case, the 2D nutation method is recommended. Further progress with this sequence should include (i) the hetero and homonuclear magnetic dipole–dipole interactions, which provide atomic distances, (ii) the second-order quadrupole interaction in order to obtain strong QCC values, and (iii) the effect of a nonzero asymmetry parameter on the line intensity. Finally, this sequence should be tested for the cancellation of piezoelectric signals.

ACKNOWLEDGMENT

We thank Dr. D. Müller (Bruker, Karlsruhe, Germany) for providing the composite-pulse sequence program for MSL spectrometers.

REFERENCES

1. A. C. Kunwar, G. L. Turner, and E. Oldfield, Solid-state spin-echo Fourier transform NMR of ^{39}K and ^{67}Zn salts at high field, *J. Magn. Reson.* **69,** 124–127 (1986).
2. I. P. Gerothanassis, Methods of avoiding the effects of acoustic ringing in pulsed Fourier transform NMR spectroscopy, *Progr. Nucl. Magn. Reson. Spectrosc.* **19,** 267–329 (1987).
3. P. P. Man, Study of a spin-3/2 system by a quadrupolar-echo sequence: Suppression of spurious signals, *Solid State NMR* **1,** 149–158 (1992).
4. D. G. Hughes and L. Pandey, Spurious signals caused by the piezoelectric ringing of $NaNO_2$ in pulsed NMR, *J. Magn. Reson.* **56,** 428–442 (1984).
5. M. E. Smith and E. R. H. van Eck, Recent advances in experimental solid state NMR methodology for half-integer spin quadrupolar nuclei, *Progr. Nucl. Magn. Reson. Spectrosc.* **34,** 159–201 (1999).
6. J. C. C. Chan, Spin echoes in half-integer quadrupole systems, *Concepts Magn. Reson.* **11,** 363–377 (1999).
7. S. Zhang, X. Wu, and M. Mehring, Elimination of the ringing effects in multiple-pulse sequences, *Chem. Phys. Lett.* **173,** 481–484 (1990).
8. Y. Dumazy, J.-P. Amoureux, and C. Fernandez, Theoretical and experimental study of quadrupolar echoes in solid state NMR, *Mol. Phys.* **90,** 959–970 (1997).
9. I. L. Moudrakovski, C. I. Ratcliffe, and J. A. Ripmeester, ^{131}Xe, a new NMR probe of void space in solids, *J. Am. Chem. Soc.* **123,** 2066–2067 (2001).
10. A. Samoson and E. Lippmaa, 2D NMR nutation spectroscopy in solids, *J. Magn. Reson.* **79,** 255–268 (1988).
11. A. P. M. Kentgens, J. J. M. Lemmens, F. M. M. Geurts, and W. S. Veeman, Two-dimensional solid-state nutation NMR of half-integer quadrupolar nuclei, *J. Magn. Reson.* **71,** 62–74 (1987).
12. A. P. M. Kentgens, A practical guide to solid-state NMR of half-integer quadrupolar nuclei with some applications to disordered systems, *Geoderma* **80,** 271–306 (1999).
13. A. P. M. Kentgens, Off-resonance nutation NMR spectroscopy of half-integer quadrupolar nuclei, *Progr. Nucl. Magn. Reson. Spectrosc.* **32,** 141–164 (1998).

14. D. Fenzke, D. Freude, T. Fröhlich, and J. Haase, NMR intensity measurements of half-integer quadrupole nuclei, *Chem. Phys. Lett.* **111,** 171–175 (1984).

15. A. Samoson and E. Lippmaa, Excitation phenomena and line intensities in high-resolution NMR powder spectra of half-integer quadrupolar nuclei, *Phys. Rev. B* **28,** 6567–6570 (1983).

16. G. Campolieti, B. C. Sanctuary, and H. B. R. Cole, Multipole theory of soft pulses in NMR of quadrupolar solids, *J. Magn. Reson.* **88,** 457–472 (1990).

17. P. P. Man, Importance of the magnetic dipolar coupling on the quadrupolar spin-echo amplitude, *J. Magn. Reson.* **100,** 157–165 (1992).

18. P. P. Man, Determination of the quadrupolar coupling constant in powdered samples with a two in-phase rf pulse sequence in solid-state NMR, *Chem. Phys. Lett.* **168,** 227–232 (1990).

19. P. P. Man, Measurement of quadrupolar spin population by solid-state NMR, *J. Magn. Reson.* **77,** 148–154 (1988).

20. D. Freude and J. Haase, Quadrupole effects in solid-state nuclear magnetic resonance, *in* "NMR Basic Principles and Progress" (P. Diehl, E. Fluck, H. Günter, R. Kosfeld, and J. Seelig, Eds.), Vol. 29, pp. 1–90, Springer-Verlag, Berlin, 1993.

21. P. P. Man, Measurement of the quadrupolar coupling with two-pulses of opposite phase, *J. Magn. Reson.* **94,** 258–267 (1991).

22. A. Wokaun and R. R. Ernst, Selective detection of multiple quantum transitions in NMR by 2D spectroscopy, *Chem. Phys. Lett.* **52,** 407–412 (1977).

23. K. Narita, J. J. Umeda, and H. Kusumoto, NMR powder patterns of the second-order nuclear quadrupole interaction in solids with asymmetric field gradient, *J. Chem. Phys.* **44,** 2719–2723 (1966).